Photonic crystal-based biosensing for TB detection

Charles Maphanga [1, 2*], Saturnin Ombinda-Lemboumba [1], Yaseera Ismail [2], Patience Mthunzi-Kufa [1, 2, 3]

[1]Council for Scientific and Industrial Research, National Laser Centre, P O BOX 395, Pretoria, 0001, South Africa
[2]University of KwaZulu-Natal, School of Chemistry and Physics, Westville Campus, University Road, Durban, South Africa
[3]Department of Human Biology, Division of Biomedical Engineering, University of Cape Town, Cape Town 7935, South Africa

E-mail: CMaphanga@csir.co.za

Abstract. Over the last three decades, biosensors based on photonic crystals (PhCs) have been developed and continue to receive significant recognition owing to their distinctive electromagnetic properties and broad applications. Studies that have used refractive index as a parameter to design optical biosensing devices based on PhCs have resulted in optical devices that are sensitive with quick response time for small variations in samples. In this study, a 1-dimensional (I-D) PhC biosensor chip was developed for the diagnosis of TB. A pathogen-specific mycolic acid (MA) TB biomarker was studied based on the detection of refractive index changes on functionalised PhC biosensing surface. The MA biomarker was used as the biorecognition element to capture anti-mycobacterium tuberculosis antibodies, and a custom-built optical biosensing setup was used for optical biosensing to monitor biomolecular interactions between the antigen and antibody. Functionalised and successfully characterised gold nanoparticles (AuNPs) were introduced on the biosensing surface to enhance the detection signal. The biosensing surface was further characterised using atomic force microscopy (AFM). Analysis of biomolecular binding events on the biosensing surface was achieved using the optical biosensing setup by measuring transmitted light through the biosensor chip, and successfully distinguishing differences between the experiment and control samples. From our findings, it was realised that mycolic acid antigen can be used as a biomarker for active TB and can be successfully immobilised on a biosensing surface to capture anti-mycobacterium tuberculosis antibodies. It was evident that the PhC-based optical biosensing technique was successful in detecting small refractive index changes on the biosensing surface for the diagnosis of TB. These results pave the way toward the development of a PhC-based point-of-care (POC) diagnostic device for TB.

1. Introduction

The PhCs are periodic nanostructures that manipulate the flow of light and have garnered significant interest in the field of biosensing with their potential application in the development of point-of-care (POC) diagnostic devices. PhC-based biosensing plays a crucial role in the development of point-of-care diagnostics. They can be engineered to exhibit strong light-matter interactions, resulting in enhanced sensitivity for detecting analytes. By tailoring the structural properties of PhCs, such as the periodicity and refractive index contrast, the interaction of light with biomolecules can be optimised, leading to increased sensitivity in detecting molecular binding events [1–3]. PhC-based biosensors

offer label-free detection, eliminating the need for fluorescent or radioactive labels [4–6]. This simplifies the assay procedure and reduces costs. The interaction of analytes with the PhC structure causes changes in the optical properties, such as the shift in the wavelength or change in intensity, enabling direct detection without the use of additional labels or probes [6].

One of the advantages of PhC-based biosensors is their capability for real-time monitoring of biomolecular interactions. The changes in the optical properties of the PhC structure occur instantaneously upon analyte binding, allowing the detection and analysis of binding kinetics and affinity [6]. Real-time monitoring enables dynamic measurements, enhancing the understanding of biomolecular interactions and enabling timely diagnostic decisions. In this work, a 1-D PhC surface was modified and used as the biosensor chip. A PhC biosensor chip was developed by immobilising the mycolic acid TB antigen surface of the PhC. Mycolic acid was used as a biorecognition element to specifically bind the anti-*mycobacterium tuberculosis* antibody as the analyte. Furthermore, gold nanoparticles (AuNPs) were covalently conjugated with a secondary antibody and introduced on the biosensing surface to enhance the detection signal. The AuNPs were characterised before and after bioconjugation using ultraviolet-visible (UV-vis) spectroscopy before introducing them on the biosensing surface. The biosensing surface was also characterised layer-by-layer during the development process of the biosensor chip using atomic force microscopy (AFM). The biosensor chip was analysed using a custom-built PhC setup, transmitted light intensity was measured, and a shift in the wavelength due to refractive index changes was detected using a spectrometer. The acquired data were analysed using OriginPro software to visualise the transmission spectra between the neat PhC, experiment, and control samples.

2. Materials and Methods

2.1. Atomic force microscopy

The AFM was used to perform layer-by-layer characterisation of the biosensing surface for surface morphology studies of the PhC biosensor chips at different stages of the functionalisation process. Herein, the 1-D PhC biosensor chip was washed with absolute ethanol and blow-dried with nitrogen (N_2) gas. The chip was subsequently subjected to oxygen plasma treatment. The PhC was immersed in (3-Aminopropyl) triethoxysilane (APTES) (1%, v/v) (Sigma-Aldrich, A3648) at room temperature overnight. Post incubation, the PhC was washed thoroughly by sonication in absolute ethanol for 5 minutes and followed by sonication in ultrapure water (resistivity of 18 MΩ) for 5 minutes. The clean PhC was blow-dried with N_2 gas and placed in the incubator at 90°C for 1 hour. The silanised PhC surface was functionalised with stearic acid (STA) (141 mM) (Sigma-Aldrich, S4745). Mycolic acid (MA) from *mycobacterium tuberculosis* (bovine strain) (0.5 mg/mL) (Sigma-Aldrich, M4537) was immobilised on the STA monolayer by incubating the chip in a solution of MA overnight at room temperature. Post incubation, the chip was rinsed thoroughly with 1x phosphate buffered saline (PBS) (Sigma-Aldrich, D1283). A solution of bovine serum albumin (BSA) (1%, v/v) (Roche Diagnostics, 10711454001) was added to the chip for an hour. Anti-*mycobacterium tuberculosis* primary antibody (8.8 mg/ml) (Abcam, ab905) added to the MA monolayer and incubated overnight. A goat anti-rabbit IgG H&L secondary antibody (2.1 mg/ml) (Abcam, ab6702) was conjugated to gold nanoparticles (AuNPs) (Sigma-Aldrich, 797707) and herein called the bioconjugate. (AuNPs-IgG) and introduced on the surface containing primary antibody. In the specifity control sample, the primary antibody was not introduced on the surface; however, the TB bioconjugate was introduced on the surface containing MA. AFM images were captured with a Vecco AFM system (Digital Instruments, USA).

2.2. Transmission electron microscopy

The morphological analysis of the AuNPs used in this study was performed using a High-Resolution Transmission Electron Microscope (HRTEM) (JEOL JEM-2100, Japan) operated at a voltage of 200 Kilovolt (KV). A copper grid was used for sample preparation and dipped into a sample of AuNPs suspended in PBS. The HRTEM operates at an imaging mode with high magnification, thus enabling

high-resolution imaging of the crystallographic structure of nanomaterials at the atomic scale level. In this analysis, the HRTEM analysis was used for analysing the morphology, particle size and shape to confirm the structural properties of the AuNPs for subsequent studies.

2.3. Ultraviolet-visible (UV-vis) absorption spectroscopy

UV-vis absorption spectroscopy was performed to characterise the gold nanoparticles (AuNPs) before and after bioconjugation. Covalent and direct bioconjugation strategies were explored. To perform covalent conjugation, N-hydroxysuccinimide (NHS) (13 mM) (Sigma-Aldrich, 56480) and 1-Ethyl-3-(3-dimethylaminopropyl)-carbodiimide) (EDC) (5 mM) (Sigma-Aldrich, E7750) with similar molar ratio were added to heterobifunctional polyethylene glycol (PEG) (SH-PEG-COOH) (Sigma-Aldrich, 757845) and shaken for an hour on an orbital shaker. Subsequently, the anti-*mycobacterium tuberculosis* antibody was introduced to the reaction mixture and incubated for 2 hours. The mixture was complex was added to 200 µL of AuNPs and incubated for an hour on an orbital shaker. To perform physical conjugation, the anti-*mycobacterium tuberculosis* antibody was added directly to 200 µL AuNPs. The mixture was incubated on an orbital shaker for 30 min. Additionally, neat AuNPs were used as a reference. Bioconjugation was confirmed by measuring the samples using NanoDrop 8000 spectrophotometer (Thermo Fisher Scientific, United States).

2.4. Photonic crystal biosensing

A custom-built optical biosensing setup with a transmission spectroscopy conformation was used to perform PhC biosensing. The setup was assembled using a broadband light-emitting diode (LED) light source. The light was collimated using a combination of collimating lenses and focused on the sample stage. Light transmitted through the PhC biosensor chip on the stage was collected using a 10x microscope objective. A 50/50 beam splitter directed the light to the imaging system and the spectrometer using a fiber. Transmitted light was focused into the fiber using a focussing lens and directed to the USB 4000 portable spectrometer (Ocean Optics Inc, United States) connected to the computer. The imaging system enabled the visualisation of biosensing activities on the sample stage and was formed by a charge-coupled device (CCD) camera connected to a computer. SpectraSuit software was used to perform spectroscopic analysis of the different samples. The samples were prepared in triplicates under the same conditions and the analysis was repeated three times ($n=3$). During sample analysis, background measurements were taken before each recording. The acquired data was further analysed using OriginPro8 software to plot wavelength-shift differences between the samples.

3. Results

3.1. Atomic force microscopy

Atomic force microscopy was used in this study to perform layer-by-layer characterisation of the PhC biosensor chip surface during the chip functionalisation process. The samples included neat PhC, control, and experiment samples. The control sample consisted of mycolic acid immobilised on the biosensing surface as the biorecognition element and the goat anti-rabbit IgG H&L secondary antibody bioconjugated to AuNPs (TB-bioconjugate). There was no primary antibody on the surface of the control sample. Mycolic acid used in this study can only bind to the anti-*mycobacterium tuberculosis* antibody, and the secondary antibody is designed to bind to the primary antibody. The experiment sample consisted of mycolic acid, an anti-*mycobacterium tuberculosis* primary antibody, and the TB bioconjugate. The images taken using AFM are shown in Figure 1, and each of the scans represents a 5µm X 5µm lateral area that was scanned.

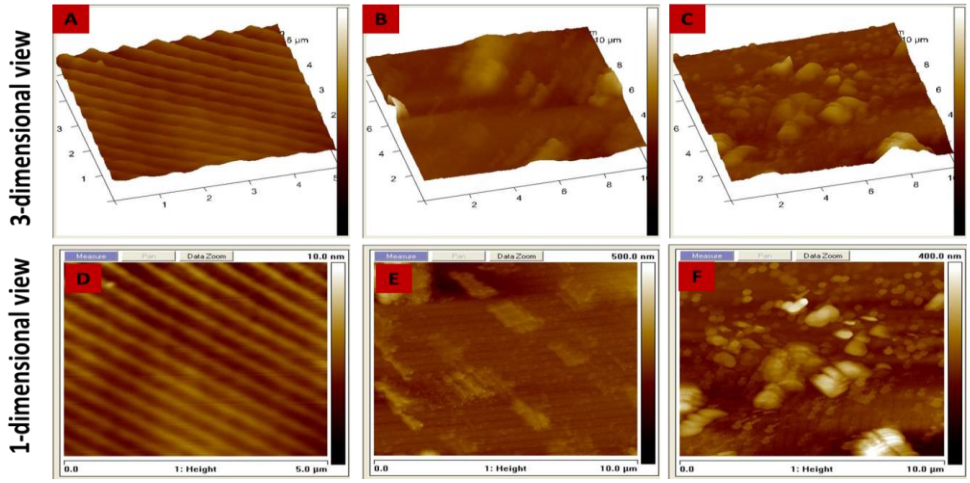

Figure 1: Atomic force microscopy micrographs of the PhC, control, and experiment group displayed in 3-dimensional and 1-dimensional view projection. Figures A and D show the 1-D PhC displayed in 3-D and 1-D view. Figures B and E show the control sample in 3-D and 1-D view projection. The experiment sample displayed much more surface roughness compared to the control sample.

Figure 1A and D shows the neat PhC surface depicting the band structure representing the periodicity of the PhC. The consistent crest and trough pattern of the PhC periodicity is represented in Figure 1A. The surface is uniform, with no signs of irregularities, defects, or contaminants. Prominent surface roughness was observed in the experiment sample (Figure 1C and F) when compared to the control sample (Figure 1B and E). The Z-range increased from 150 nm in the neat 1-D PhC sample used as a reference to 344 nm in the control sample. The experiment sample containing immobilised bioconjugated AuNPs displayed a z-range of 473 nm.

3.2. Transmission electron microscopy

The morphology and size of AuNPs were evaluated. Figure 2 shows the TEM image of bare AuNPs, specifically Au NanoUrchins used in this study. Under TEM analysis, the AuNPs appeared multi-branched with spiky, uneven surfaces. The AuNPs had an average size of 60 nm.

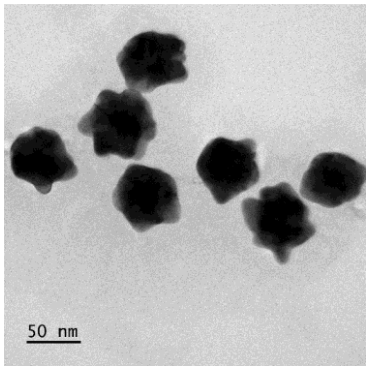

Figure 2: Transmission electron micrograph of gold NanoUrchins. The nanoparticles displayed a multibranched, spiky, uneven surface morphology with an average size of 60nm. The length of the scale bar is 50nm.

3.3. UV-vis absorption spectroscopy

To characterise the AuNPs before and after bioconjugation using covalent conjugation chemistry and physical conjugation, UV-vis absorption spectroscopy was performed (Figure 3). At A250 nm – 350 nm, there is no absorption peak for the AuNPs. At A250 nm – 350 nm, the high absorption intensity of antibodies physically conjugated (TB-Bioconjugate-P) to the AuNPs was detected, and lower absorption intensity was recorded for the covalently bioconjugated antibodies (TB-Bioconjugate-C). At A500 nm – 750 nm, approximately 645 nm absorbance peak for the AuNPs was detected, and a redshift in both the covalent and physically conjugated AuNPs was detected. In this region, a notable difference in absorbance intensity was also recorded between the AuNPs, TB-Bioconjugate-P, and TB-Bioconjugate-C.

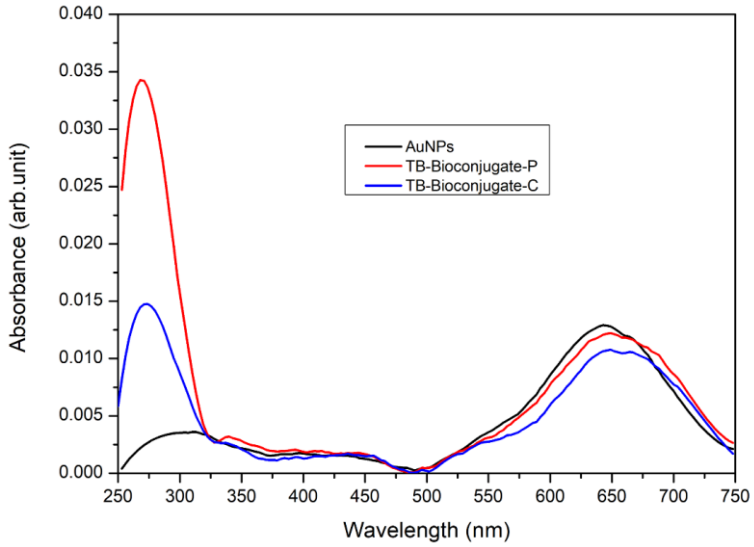

Figure 3: Absorbance spectra of neat AuNPs, covalent conjugated AuNPs (TB-Bioconjugate-C), and physical bioconjugated AuNPs (TB-Bioconjugate-P). There are clear differences in absorbance intensity of the antibody (A250 nm – 350 nm) and the AuNPs (A500 nm – 750 nm) when comparing the two bioconjugation techniques.

3.4. Photonic crystal biosensing

A custom-built PhC biosensing setup was used to differentiate and detect differences between the neat 1-D PhC, MA, MA with immobilised primary antibody (PAb), MA with immobilised PAb and bioconjugated secondary antibody (SAb), and MA with immobilised bioconjugated SAb (Figure 4). Transmitted light intensity was measured between the five samples. There were clear resonance wavelength-shift differences between the samples analysed. The neat PhC reference sample (herein referred to as the reference sample) was detected at a resonance wavelength of 650.08 nm, which corresponds to the manufacturer's recommendations. The MA sample was detected at a wavelength of 653.28 nm, MA with immobilised PAb was detected at a wavelength of 660.27 nm, MA with immobilised PAb and bioconjugated SAb was detected at 664.45 nm, and MA with immobilised SAb (herein referred to as the control sample for specificity) was detected at 653.28 nm. A redshift of 3.2 nm was detected when MA was compared to the reference sample, a redshift of 14.37 nm was detected when the sample containing immobilised PAb (herein referred to as the experiment sample) was compared to the reference sample, a redshift of 10.19 nm was detected when the sample containing MA/PAb and AuNPs bioconjugated SAb (herein referred to as the signal enhancement sample) was compared to the reference, and a redshift of 6.8 nm was detected when the sample containing AuNPs bioconjugated SAb (herein referred to as the specificity control sample) was compared to the reference sample. Additionally, a blueshift of 11.17 nm was detected between the specificity control sample and the experiment sample.

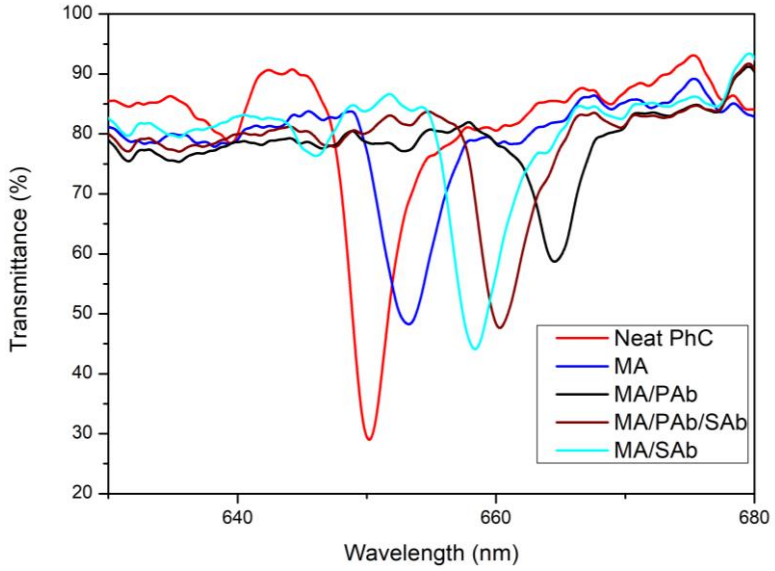

Figure 4: Photonic crystal spectrograph for the detection of anti-*mycobacterium tuberculosis* antibodies. The resonance wavelength of neat 1-D photonic crystal (PhC), mycolic acid (MA) mycolic acid with immobilised primary antibody (PAb), MA with immobilised PAb and bioconjugated secondary antibody (SAb), and MA with immobilised bioconjugated SAb was obtained using the custom-built PhC biosensing setup. There were clear detectable resonance wavelength differences between the five samples.

4. Discussion

The PhC-based biosensing surface was characterised layer-by-layer using AFM during the surface functionalisation process to confirm the binding of molecules on the surface. Immobilisation of molecules on the biosensing surface was achieved through covalent attachment and the formation of self-assembled monolayers. Samples, including the neat PhC, control, and experiment, were studied. The neat PhC was used as the reference sample. A biorecognition element (MA) was immobilised on both the control and experiment samples. However, a complementary PAb was not introduced on the surface of the control sample, but rather a bioconjugated SAb was introduced to both the control and experiment samples. In the control, the bioconjugate was used to test for the specificity of the biorecognition element. In the absence of a primary antibody on the surface of the control sample, the prominent surface roughness observed in the experiment sample (Figure 1C and F) was not detected (Figure 1B and E). Various structures resembling AuNP-antibody complexes were visualised in Figures 1C and F of the experiment sample. This also supports findings by Lee et al., 2015 who demonstrated the possibility of visualising AuNP-antibody complexes as a result of the presence of immobilised AuNPs. The increased surface roughness in the experiment sample could be attributed to the immobilisation of the AuNPs contained in the bioconjugate bound to the experiment sample. This is also supported by the Z-range values of 150 nm in the neat 1-D PhC sample, 344 nm in the control sample, and 473 nm in the experiment sample. This can be an indication that the immobilisation of the SAb to the AuNPs was successful, and further attached to the PAb in the experiment sample.

On TEM, the AuNPs appeared multibranched with a spiky uneven surface. Multibranched and spiky AuNPs have a highly porous and rough surface structure, providing a significantly larger surface area compared to their spherical counterparts [8]. This increased surface area allows efficient immobilisation of biomolecules, leading to enhanced sensitivity in biosensing applications. The larger surface area also results in improved binding affinity, thus improving the detection limits of the biosensor [8]. The unique surface morphology of multibranched and spiky AuNPs can lead to signal amplification in biosensing. The presence of multiple branches or spikes on the nanoparticles creates

numerous nanogaps, which can trap and amplify the signal produced during the sensing process. This amplification effect enhances the detection sensitivity and improves the signal-to-noise ratio of the biosensor [8–10].

The AuNPs were further functionalised with a signal or secondary antibody using both the covalent and physical bioconjugation techniques. Bioconjugation occurs upon successful binding of the antibodies to the AuNPs surface, thus resulting in LSPR spectrum redshift which is an increase in wavelength by a few nanometres [11]. From the findings, it was realised that covalent conjugation resulted in high binding efficiency of antibodies to the surface of the AuNPs indicated by the sharp decline in the absorption intensity of the antibodies at A250 nm – 350 nm and a redshift in the wavelength at A500 nm – 750 nm (Figure 3). The physical conjugation strategy resulted in lower binding efficiency of antibodies to AuNPs indicated by the high absorbance intensity of the antibodies at A250 nm – 350 nm, and a less prominent redshift in the wavelength at A500 nm – 750 nm (Figure The AuNPs do not absorb at A250 nm – 350 nm; hence no absorption peak was detected.

After the characterisation of the biosensing surface, PhC-based biosensing of the chip was performed using the custom-built optical biosensing setup. During analysis, wavelength shift between the samples was studies. There were distinct differences in wavelength redshift between the five samples analysed. The redshift detection is due to changes in the refractive index between samples [12]. The reference sample (neat PhC) exhibited a resonance wavelength of 650.08 nm, consistent with the manufacturer's specifications. Notably, the MA sample demonstrated a redshift of 3.2 nm compared to the reference, while the introduction of immobilised PAb led to a larger redshift of 14.37 nm, marking the experiment sample and a positive TB sample in diagnostics. Further modifications involving the incorporation of AuNPs bioconjugated SAb onto the MA/PAb structure resulted in a redshift of 10.19 nm when compared to the reference sample. However, this shift was not greater than the one detected in the absence of the bioconjugate (14.37 nm). This indicates the possibility of detecting anti-*mycobacterium tuberculosis* antibodies without the introduction of nanomaterials. Additionally, the specificity control sample involving AuNPs bioconjugated SAb showed a redshift of 6.8 nm relative to the reference, serving as a benchmark for specificity. Moreover, a notable blueshift of 11.17 nm emerged when comparing the specificity control sample (MA/SAb) to the experiment sample (MA/PAb). Overall, the differences in resonance wavelength shifts across the various samples provide valuable information and a diagnostic foundation that can be used to distinguish between negative and positive TB samples, offering potential implications for sensor development for TB diagnostics. These findings suggest a possible diagnosis of TB using a label-free PhC optical biosensing platform, and further exploration in this direction could lead to advancements in bioanalytical techniques and sensor design.

5. Conclusion

In conclusion, the study successfully detected anti-*mycobacterium tuberculosis* antibodies using a 1D photonic crystal-based biosensor chip. Mycolic acid was effectively immobilised on the biosensor chip to facilitate specific binding to anti-*mycobacterium tuberculosis* antibodies. To rule out non-specific binding, a bioconjugated secondary antibody was introduced, which did not bind to the biorecognition element, and this was confirmed using atomic force microscopy (AFM). AFM also revealed distinct differences in height and surface roughness among the samples studied. The bioconjugated secondary antibody was successfully bound to the primary antibody on the biosensing surface, inducing a change in surface refractive index. Additionally, the developed custom-built PhC optical biosensing setup enabled the detection of refractive index changes through wavelength shifts between the five samples studied. The observed redshifts in resonance wavelengths across various samples were indicative of specific binding interactions. The distinct spectral responses and shifts provide a significant diagnostic foundation for the detection of negative and positive TB specimens. These findings collectively suggest the promising prospect of diagnosing tuberculosis using the label-free PhC optical biosensing platform. Subsequent studies will focus on the reproducibility of the assay for label-free detection and the limit of detection studies.

References

[1] H. Wang, K.Q. Zhang, Photonic crystal structures with tunable structure color as colorimetric sensors, Sensors (Switzerland). 13 (2013) 4192–4213. https://doi.org/10.3390/s130404192.

[2] V.N. Konopsky, T. Karakouz, E. V. Alieva, C. Vicario, S.K. Sekatskii, G. Dietler, Photonic crystal biosensor based on optical surfacewaves, Sensors (Switzerland). 13 (2013) 2566–2578. https://doi.org/10.3390/s130202566.

[3] O. Tokel, F. Inci, U. Demirci, Advances in plasmonic technologies for point of care applications, Chem. Rev. 114 (2014) 5728–5752. https://doi.org/10.1021/cr4000623.

[4] E. Luan, H. Shoman, D.M. Ratner, K.C. Cheung, L. Chrostowski, Silicon photonic biosensors using label-free detection, Sensors (Switzerland). 18 (2018) 1–42. https://doi.org/10.3390/s18103519.

[5] B.T. Cunningham, M. Zhang, Y. Zhuo, L. Kwon, C. Race, Recent Advances in Biosensing with Photonic Crystal Surfaces: A Review, IEEE Sens. J. 16 (2016) 3349–3366. https://doi.org/10.1109/JSEN.2015.2429738.

[6] D. Dorfner, T. Zabel, T. Hürlimann, N. Hauke, L. Frandsen, U. Rant, G. Abstreiter, J. Finley, Photonic crystal nanostructures for optical biosensing applications, Biosens. Bioelectron. 24 (2009) 3688–3692. https://doi.org/10.1016/j.bios.2009.05.014.

[7] J.H. Lee, B.C. Kim, B.K. Oh, J.W. Choi, Highly sensitive electrical detection of HIV-1 virus based on scanning tunneling microscopy, J. Nanosci. Nanotechnol. 15 (2015) 1117–1122. https://doi.org/10.1166/jnn.2015.9336.

[8] S. Stassi, V. Cauda, G. Canavese, D. Manfredi, I. Roppolo, P. Martino, Handbook of Nanomaterials Properties, 2014. https://doi.org/10.1007/978-3-642-31107-9.

[9] Y. Zou, H. Chen, Y. Li, X. Yuan, X. Zhao, W. Chen, F. Cao, N. Cai, X. Huang, F. Yang, W. Liu, Synthesis of mesoporous-silica coated multi-branched gold nanoparticles for surface enhanced Raman scattering evaluation of 4-bromomethcathinone, J. Saudi Chem. Soc. 23 (2019) 378–383. https://doi.org/10.1016/j.jscs.2018.11.005.

[10] M. He, B. Cao, X. Gao, B. Liu, J. Yang, Synthesis of multi-branched gold nanostructures and their surface-enhanced Raman scattering properties of 4-aminothiophenol, J. Mater. Res. 34 (2019) 2928–2934. https://doi.org/10.1557/jmr.2018.503.

[11] J.P. Oliveira, A.R. Prado, W.J. Keijok, P. Wagnner, P. Antunes, E.R. Yapuchura, M. Cesar, C. Guimarães, Impact of conjugation strategies for targeting of antibodies in gold nanoparticles for ultrasensitive detection of 17 β -estradiol, Sci. Rep. 9 (2019) 1–8. https://doi.org/10.1038/s41598-019-50424-5.

[12] C. Maphanga, S. Manoto, S. Ombinda-lemboumba, Y. Ismail, Localized surface plasmon resonance biosensing of Mycobacterium tuberculosis biomarker for TB diagnosis, Sens. Bio-Sensing Res. 39 (2023) 100545. https://doi.org/10.1016/j.sbsr.2022.100545.